# Substrate-Assisted Self-Organization of Radial $\beta$-AgVO$_3$ Nanowire Clusters for High Rate Rechargeable Lithium Batteries

Chunhua Han,[†,§] Yuqiang Pi,[†,§] Qinyou An,[†] Liqiang Mai,*[,†,‡] Junlin Xie,[†] Xu Xu,[†] Lin Xu,[†,‡] Yunlong Zhao,[†] Chaojiang Niu,[†] Aamir Minhas Khan,[†] and Xiaoyun He[†]

[†]State Key Laboratory of Advanced Technology for Materials Synthesis and Processing, WUT-Harvard Joint Nano Key Laboratory, School of Materials Science and Engineering, Wuhan University of Technology, Wuhan 430070, China
[‡]Department of Chemistry and Chemical Biology, Harvard University, Cambridge, Massachusetts 02138, United States

Ⓢ *Supporting Information*

**ABSTRACT:** Rational assembly of unique complex nanostructures is one of the facile techniques to improve the electrochemical performance of electrode materials. Here, a substrate-assisted hydrothermal method was designed and applied in synthesizing moundlily like radial $\beta$-AgVO$_3$ nanowire clusters. Gravitation and F$^-$ ions have been demonstrated to play important roles in the growth of $\beta$-AgVO$_3$ nanowires (NWs) on substrates. The results of cyclic voltammetry (CV) measurement and X-ray diffraction (XRD)



characterization proved the phase transformation from $\beta$-AgVO$_3$ to Ag$_{1.92}$V$_4$O$_{11}$ during the redox reaction. Further electrochemical investigation showed that the moundlily like $\beta$-AgVO$_3$ nanowire cathode has a high discharge capacity and excellent cycling performance, mainly due to the reduced self-aggregation. The capacity fading per cycle from 3rd to 51st is 0.17% under the current density of 500 mA/g, which is much better than 1.46% under that of 20 mA/g. This phenomenon may be related to the Li$^+$ diffusion and related kinetics of the electrode. This method is shown to be an effective and facile technique for improving the electrochemical performance for applications in rechargeable Li batteries or Li ion batteries.

**KEYWORDS:** Substrate-assisted hydrothermal method, moundlily like $\beta$-AgVO$_3$ nanowires, electrochemical performance, rechargeable lithium batteries, high rate performance
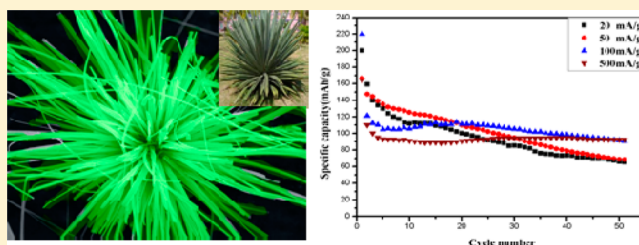
Nanostructures, especially nanowires, have received great interest and been widely applied in a variety of fields, such as electronics, optoelectronics, electrochemistry, and so forth.[1−10] Among them, the electrochemical energy storage of the Li battery or Li-ion battery (LIB) is one of the most important applications, because of their high energy density and excellent cycling lifetime.[11−15] It is worth noting that the storage of the Li batteries or LIBs at a high charge and discharge rate is an important technology in today's society.[16] However, nanomaterials often suffer from the self-aggregation in their applications, which may reduce the effective contact areas of active materials, conductive additives, and electrolytes. Assembling the complex nanostructures such as porous nanostructures, ultralong hierarchical nanowires, and kinked nanowires can reduce the self-aggregation to ensure the large effective contact areas.[17−22] The moundlily is a plant whose branches are separated naturally and hard to twist together even in harsh conditions. Therefore, if biomimic moundlily like nanowires are formed, self-aggregation can be effectively prevented. Such a nanostructure is relatively favorable for electrode materials of high-performance Li batteries or LIBs.

Owning to their unique physicochemical properties, vanadium oxides and vanadium oxide related compounds have gained more and more interest in many fields, such as electrochromic devices, lithium batteries, catalysts, gas sensors,

and so forth.[23,24] Silver vanadium oxides (SVOs),[25,26] especially $\beta$-AgVO$_3$, have drawn much attention due to its higher Ag:V molar ratio and better high-rate discharge capacity.[27,28] Song et al. synthesized superlong $\beta$-AgVO$_3$ nanowires by a pyridine-assisted solution approach and studied its electrochemical performance.[29] Mai et al. designed and successfully synthesized $\beta$-AgVO$_3$/polyaniline (PANI) triaxial nanowires by combining in situ chemical oxidative polymerization, which exhibited enhanced electrochemical performance.[30]

Here we demonstrated a substrate-assisted hydrothermal approach to synthesize moundlily like $\beta$-AgVO$_3$ nanowires on substrates and demonstrated that the gravitation and the presence of F$^-$ are essential to precipitate the precursor, which can lead to a robust mechanical adhesion between the final product and the substrate. During the charge−discharge process, $\beta$-AgVO$_3$ is transformed to Ag$_{1.92}$V$_4$O$_{11}$ which can be confirmed by cyclic voltammetry (CV) measurement and X-ray diffraction (XRD) characterization. Moreover, it was found that $\beta$-AgVO$_3$ displayed better cycling stability at a higher discharge
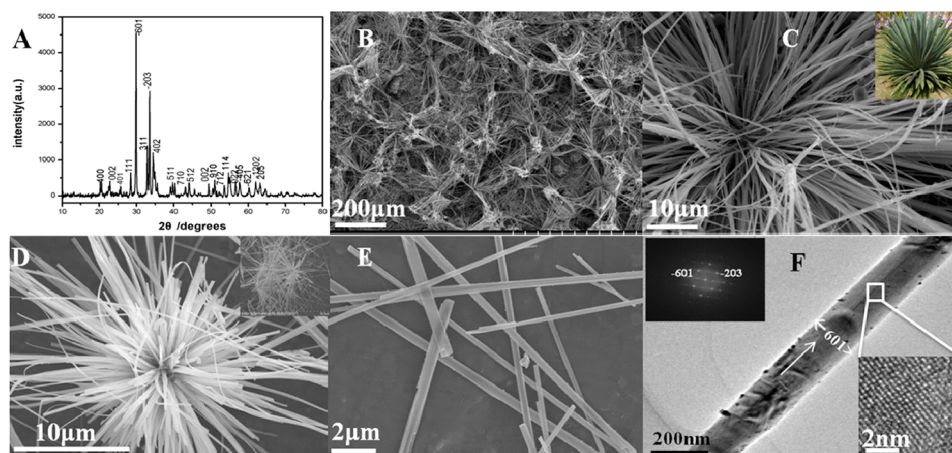
**Figure 1.** (A) XRD pattern of $\beta$-AgVO$_3$ grown on the ITO substrate. (B, C) SEM images of $\beta$-AgVO$_3$ grown on the ITO substrate, the real moundlily shown in the inset of C. (D) SEM image of $\beta$-AgVO$_3$ in the solution of autoclave. (E) SEM image of $\beta$-AgVO$_3$ synthesized without substrate. (F) TEM image and FFT pattern of $\beta$-AgVO$_3$ on the ITO substrate.
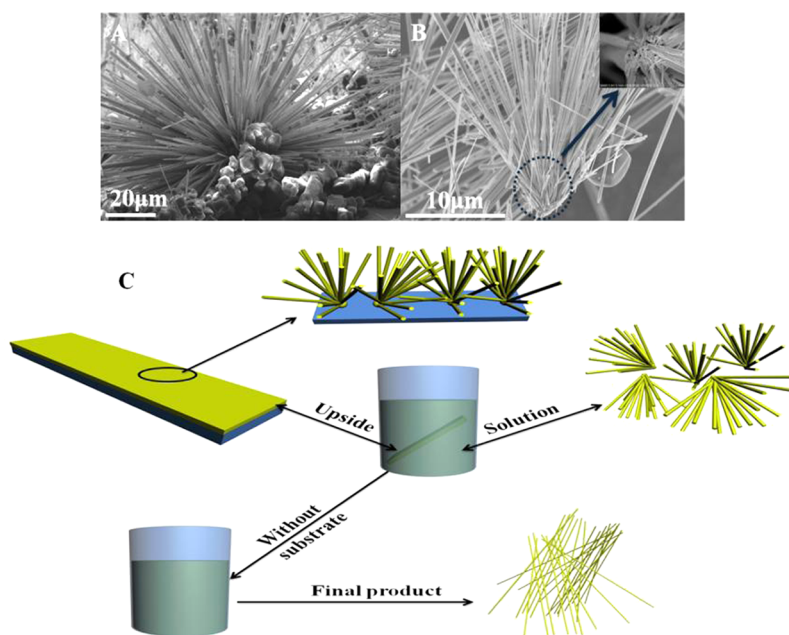


**Figure 2.** (A, B) SEM images of $\beta$-AgVO$_3$ on ITO substrate and in autoclave separately. (C) Schematic mechanism for the different growth process of one-dimensional $\beta$-AgVO$_3$ grown on the up side of substrate and in the autoclave.

current density, which may be attributed to the direct pathways of Li$^+$ diffusion.

The moundlily like $\beta$-AgVO$_3$ nanowires grown on an ITO (tin-doped indium oxide) conductive substrate were synthesized by adding 0.1699 g of AgNO$_3$, 0.0909 g of V$_2$O$_5$, and 0.0778 g of LiF in a 100 mL Teflon autoclave, filled with 60 mL of deionized H$_2$O. Then, an ITO conductive substrate (sequentially cleaned with alcohol, acetone, and deionized water) was inclined in the autoclave with an angle about 45°. The autoclave was heated for 24 h at 180 °C and cooled to room temperature. Then the product was successfully obtained after filtering, washing, and drying. To demonstrate the effect of substrate on the product, the same amount of reactants added into the autoclave and heated at the same reaction conditions without any substrate. Moreover, a hydrothermal method was used to synthesize $\beta$-AgVO$_3$ nanowires as control experiment by adding 0.1699 g of AgNO$_3$ and 0.1171 g of NH$_4$VO$_3$ into the autoclave, which was also heated for 24 h at 180 °C.

The crystallographic information of the final product was examined by using a D/MAX-III X-ray diffractometer with graphite-monochromatized Cu K$\alpha$ radiation. Field emission scanning electron microscopic (FESEM) images were obtained with a Hitachi S-4800 at an acceleration voltage of 10 kV. Transmission electron microscopic (TEM) and high-resolution transmission electron microscopic (HRTEM) images were also recorded by using a JEM-2100F STEM/EDS microscope.

The electrochemical performance was studied in a potential range of 4.0−1.5 V versus Li/Li$^+$ with a multichannel battery testing system (LAND CT2001A). $\beta$-AgVO$_3$ NWs synthesized with AgNO$_3$, V$_2$O$_5$, and LiF were peeled off from ITO substrate to fabricate Li batteries. Batteries were assembled of 2025 coin cells in a glovebox filled with pure argon gas, using lithium pellet as the anode, 1 M solution of LiPF$_6$ in ethylene carbon (EC)/dimethyl carbonate (DMC) as an electrolyte. Cathode electrodes were made by grinding together 70% $\beta$-AgVO$_3$ nanowire active material, 20% acetylene black, and 10%
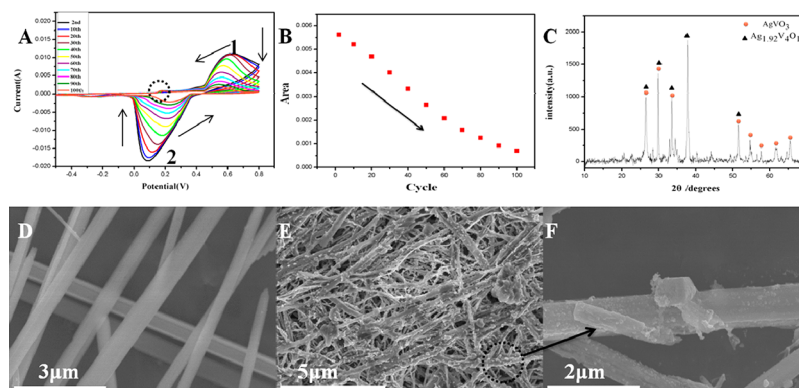
**Figure 3.** (A) CV curve of $\beta$-AgVO$_3$ grown on ITO substrate. (B) the curve of area−cycle of CV test. (C) XRD pattern of $\beta$-AgVO$_3$ on ITO substrate after 100 cycles of CV test. (D) Untested $\beta$-AgVO$_3$ nanowires. (E, F) SEM images of $\beta$-AgVO$_3$ after CV test.

poly(tetrafluoroethylene). CVs were tested with an electrochemical workstation (CHI 760D).

In Figure 1A, the XRD pattern shows that the product grown on the ITO substrate is monoclinic $\beta$-AgVO$_3$. All diffraction peaks can be indexed to the phase of $\beta$-AgVO$_3$ with monoclinic structure space group: $Cm$ (No. 8), PDF Card No. 01-086-1154. The (−601) diffraction peak is the strongest one, while the strongest peak of $\beta$-AgVO$_3$ powders as reported is the (311),[31] indicating the preferential orientation of the $\beta$-AgVO$_3$ nanowires.

The SEM images of $\beta$-AgVO$_3$ grown on the ITO conductive substrate are shown in Figure 1B and C, respectively, which obviously present the moundlily like shape of $\beta$-AgVO$_3$ with a relatively high density. In addition, to prove that substrate-assisted hydrothermal method is not only limited in ITO substrate, glass substrate was applied in this method. It is found that such morphology of $\beta$-AgVO$_3$ grown on the glass substrate can be also found, and the SEM images are exhibited in the Supporting Information (Figure S2). Figure 1D shows the morphology of $\beta$-AgVO$_3$ collected from the solution. Thus, we can conclude that $\beta$-AgVO$_3$ collected on the substrate and in the solution almost have the identical morphology. The SEM image of the product synthesized without any substrate is presented in Figure 1E. Although the product exhibits the nanowire morphology, it is totally different from the moundlily like shape. The TEM image of the product is shown in Figure 1F. The diameter of single $\beta$-AgVO$_3$ nanowire is about 150 nm. From the fast Fourier transform (FFT) pattern, the diffraction spots match well with the [−601] lattice direction. A typical photograph of large-scale uniform $\beta$-AgVO$_3$ nanowires grown on an ITO conductive substrate is given in the Supporting Information (Figure S1).

To demonstrate and explain the growth process, NH$_4$F has been used as the substitution of LiF for the control experiment. Though the fluorine sources are different, the experiment results turn out to be the same (Supporting Information, Figure S3A, B). Additionally, another experiment was carried out without any fluorine source, and consequently nothing grew on the ITO conductive substrate, revealing that F$^−$ is closely associated with the adhesion between substrates and the product film.[32,33] Moreover, the crystallographic information of the product at the bottom of the autoclave has been accessed, and the result showed that it is Ag$_2$V$_4$O$_{11}$, instead of $\beta$-AgVO$_3$ (Supporting Information, S4). There is an interesting phenomenon that the uniform thin film of $\beta$-AgVO$_3$ with novel 1D architecture only grows on the up side of the

substrates, while nothing can be observed on the bottom side. This phenomenon may result from the gravitation effect.

Figure 2A and B shows the SEM images of $\beta$-AgVO$_3$ on the ITO substrate and in the solution, respectively. As mentioned above, they have the similar moundlily like morphology. The growth schematic of $\beta$-AgVO$_3$ nanowires on the ITO substrate is given based on these SEM images. In fact, the ITO substrate serves as a barrier for the deposition of V$_2$O$_5$ particles, and those particles initially form a seed layer on the upside of the substrate due to gravitation. At the same time, the existence of F$^−$ enhances the mechanical adhesion between the seed layer and the substrate. The seed layer is successfully formed on the substrate due to the synergistic effect of gravitation and F$^−$. After the formation of the seed V$_2$O$_5$ layer, the seeds serve as the "growth spot", to start reaction with other reactants. However, because of the substrate's obstruction function, the nanowire growth only happens on the upside of substrate. Thus, we can see that the nanowires present the radial growth based on the spot. Moreover, as some product may peel off from the substrate during this process, the similar morphology was found at the bottom of autoclave, which was mentioned above. If there is no substrate inclined in the autoclave, the growth of $\beta$-AgVO$_3$ may be a splitting process, leading to the simple random nanowire morphology.[28,34]

To investigate the detailed electrochemical performance of $\beta$-AgVO$_3$, CV tests of $\beta$-AgVO$_3$ on the ITO conductive substrate were performed. The voltammograms were measured in 1 mol/L LiNO$_3$ aqueous solution at a sweep rate of 1 mV/s in a potential range from 0.8 to −0.5 V versus saturated calomel electrode (SCE) at room temperature. CV results of the product on the ITO conductive substrate are shown in Figure 3A. From the curve, it can be seen that the peak positions of all 100 cycles are similar. Apparently, there exists an anode peak 1 (at ca. 0.6 V) and a cathodic peak 2 (at ca. 0.2 V) on the curve, which could be designated to two reversible redox couples: Ag$^+$/Ag$^0$ and VO$^{2+}$/V$^{2+}$.[29] Noticeably, peaks 1 and 2 in all cyclic voltammogram drop gradually with the increasing cycle numbers. The area-cycle curve (Figure 3B), calculated from Figure 3A, is also in agreement with the result above. There are mainly two reasons accounting for the result. One is that the product deposited on the ITO conductive substrate gradually drops with the increasing cycle numbers, and the phenomenon is in agreement with other group's work.[29] The other reason is that the activity of material on conductive substrate degrades and the structure is destroyed during cycling process. At the same time, the positions of peaks 1 and 2 have slightly changed,
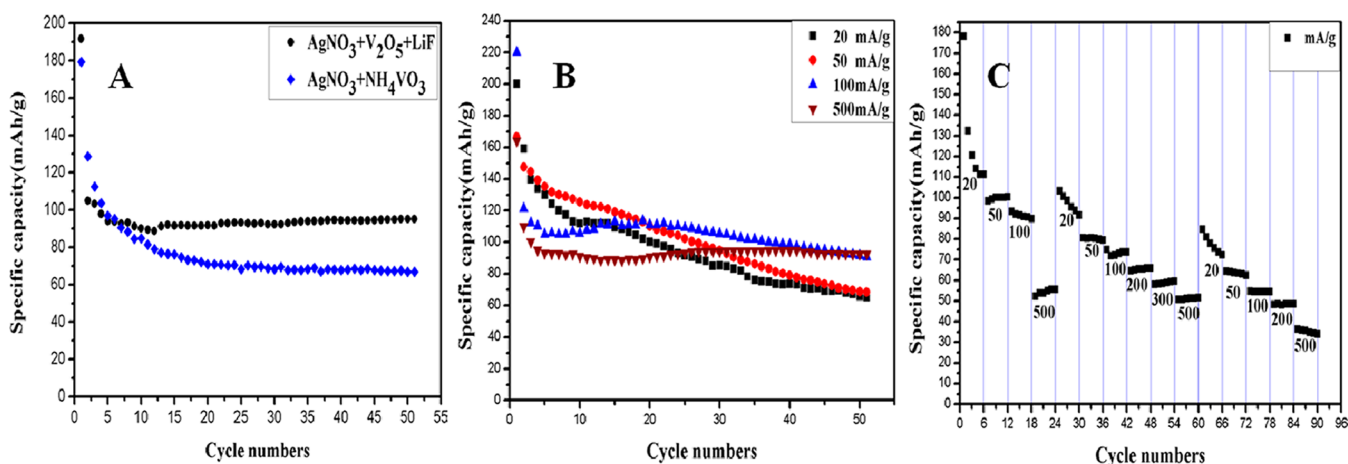
**Figure 4.** (A) Capacity vs cycle number of β-AgVO₃ nanowire cathode synthesized with different reactants. (B) Capacity vs cycle number of β-AgVO₃ nanowire cathode at different current densities. (C) The battery of β-AgVO₃ nanowire cathode was discharged at different rates from 20 mA/g to 500 mA/g.

and the redox peaks are close to each other gradually. The overpotential theory can explain the gap decreasing of redox peaks.[35,36] Besides, there exists a very small peak at ca. 0.2 V, which was related to the ITO substrate.

After 100 cycles of CV tests, the XRD and SEM tests were carried out on the β-AgVO₃ nanowires grown on the substrate. From Figure 3C, a new phase of Ag$_{1.92}$V₄O$_{11}$ can be found, indicating the phase change in charge−discharge process. Compared with the smooth surface of untested β-AgVO₃ nanowires grown on ITO substrate (Figure 3D), the morphology of SVO (shown in Figure 3E and F) after the CV test was significantly rougher, and it is estimated that those large quantities of particles on β-AgVO₃ nanowires are Ag$_{1.92}$V₄O$_{11}$ transformed from β-AgVO₃.

To investigate the influence of ITO substrate on electrochemical property, we did the CV test of an independent ITO substrate (Supporting Information, Figure S5A−F). The value of CV curve area is about $3 \times 10^{-6}$, and for the ITO substrate with β-AgVO₃ film, the value of CV curve area increases to about $5 \times 10^{-3}$, 3 orders of magnitude larger than that of bare ITO substrate; thus the influence of ITO substrate can be ignored. Moreover, an additional peak is observed in the CV curve of the independent ITO substrate, which can confirm that the additional peak observed in CV curve of β-AgVO₃ on ITO conductive substrate is caused by the ITO substrate.

Figure 4A displays the electrochemical performance of β-AgVO₃ with different morphology nanowire cathodes tested at the current density of 500 mA/g. It is apparent that the moundlily structured β-AgVO₃ nanowires from ITO substrate show a higher discharge capacity and better cycling performance than that of β-AgVO₃ nanowires synthesized with AgNO₃ and NH₄VO₃ (Supporting Information, Figure S6). The phenomenon may be attributed to several reasons. It is highly believed that the main reason is that the self-aggregation is reduced due to the existence of the moundlily nanostructure. The high surface energy of nanoscaled electrode materials is a reason for self-aggregation, which may reduce the effective contact areas of active materials, conductive additives, and electrolytes. Interestingly, the structure of moundlily like β-AgVO₃ nanowires can effectively avoid this drawback and reduce the self-aggregation, leading to better electrochemical performance. In addition, chemical lithiation may provide the contribution to improve the electrochemical of β-AgVO₃.

Chemical lithiation is often considered as an effective way to increase the cycling stability of electrode materials,[37−39] because of the fact that it can stabilize the nanostructure and improve the conductivity of host material.[40,41] In this paper, LiF was added into autoclave to help the growth of β-AgVO₃ on ITO substrate, which may also improve the cycling stability of β-AgVO₃ owning to chemical lithiation.

The performance of moundlily like β-AgVO₃ nanowires under different current densities of 20, 50, 100, and 500 mA/g are shown in Figure 4B, respectively. It can be seen that, at higher current densities, the electrochemical performances are better. When β-AgVO₃ was tested at 20 mA/g, the capacity fading per cycle was 1.46%. However, the cycle numbers-specific capacity curve shows that the capacity fading per cycle is only 0.17% at 500 mA/g, indicating the prominent cycling stability of β-AgVO₃ at high discharge current.

Considering the kinetics of electrode material, the equation ($\tau = L^2/2D$) is given, where $\tau$ is the diffusion time, $L$ is the diffusion distance, and $D$ is the Li ion chemical diffusion coefficient.[42,43] When electrode material is charged and discharged deeply at low current density, the diffusion time ($\tau$) is longer than that at high current density, which causes the specific capacity for initial several cycles is higher at low current density. But, at the same time, it is also inevitable to cause the volume expansion of the electrode materials and the structure degradation. With the increasing cycle numbers, the discharge capacity is fading particularly fast. However, when electrode material is charged and discharged at high current density, the intercalation/deintercalation of Li⁺ occurs near the surface of the electrode material; namely, the Li⁺ diffusion distance is much shorter, which leads to the increasing kinetics performance and keeps the structure stable. Although the capacity of initial several cycles is low, the cycling stability of electrode material is much better than that at low current density.

To further verify the conclusion above, the battery is discharged at different rates ranging from 20 mA/g to 500 mA/g (Figure 4C). Remarkably, the specific capacity of β-AgVO₃ always presents the decreasing trend, when it was discharged at the current density of 20 mA/g. However, the discharge capacities of the material at higher density remains stable. The phenomenon is also shown in the following two cycles, which confirms that β-AgVO₃ nanowires present better cycling stability at the higher current density. This result is in

agreement with Figure 4B, which can be attributed to the shallow charge/discharge at the higher current density, leading to the less structure damage. As a result, the active site and lithium ion pathway would still be available in the following cycle.

In summary, a facile hydrothermal method is developed to synthesize radial $\beta$-AgVO$_3$ nanowire clusters, which may be the first time to achieve large-scale $\beta$-AgVO$_3$ nanowire films directly on an ITO conductive substrate by controlling the initial reactant type. According to the results, the introduction of F$^-$ is the dominant factor to determine the $\beta$-AgVO$_3$ growth on ITO conductive substrate. Compared with the electrochemical performance of $\beta$-AgVO$_3$ with different morphology, moundlily like $\beta$-AgVO$_3$ nanowires show higher discharge capacity and better cycling performance, which may be mainly attributed to the effect of reduced self-aggregation. Moreover, $\beta$-AgVO$_3$ at a high-rate discharge exhibits excellent cycling stability, making it a promising cathode candidate in the field of energy storage devices. Significantly, this preparation is quite convenient for constructing film devices without any extra electrode preparation process and promotes the development of film devices.

## ■ ASSOCIATED CONTENT

### Ⓢ Supporting Information

Figures showing substrate photographs, SEM images, XRD patterns, and CV curves. This material is available free of charge via the Internet at http://pubs.acs.org.

## ■ AUTHOR INFORMATION

### Corresponding Author
*E-mail: mlq518@whut.edu.cn; mlq@cmliris.harvard.edu.

### Author Contributions
§These authors contributed equally to this work.

### Notes
The authors declare no competing financial interest.

## ■ ACKNOWLEDGMENTS

## ■ REFERENCES

(1) Xia, Y. N.; Yang, P. D.; Sun, Y. G.; Wu, Y. Y.; Mayers, B.; Gates, B.; Yin, Y. D.; Kim, F.; Yan, H. Q. One-Dimensional Nanostructures: Synthesis, Characterization, and Applications. *Adv. Mater.* **2003**, *15*, 353−389.

(2) Tian, B. Z.; Zheng, X. L.; Kempa, T. J.; Fang, Y.; Yu, N. F.; Yu, G. H.; Huang, J. L.; Lieber, C. M. Coaxial Silicon Nanowires as Solar Cells and Nanoelectronic Power Sources. *Nature* **2007**, *449*, 885−890.

(3) Javey, A.; Nam, S. W.; Friedman, R. S.; Yan, H.; Lieber, C. M. Layer-by-Layer Assembly of Nanowires for Three-Dimensional, Multifunctional Electronics. *Nano Lett.* **2007**, *7*, 773−777.

(4) Xu, S.; Qin, Y.; Xu, C.; Wei, Y. G.; Yang, R. S.; Wang, Z. L. Self-Powered Nanowire Devices. *Nat. Nanotechnol.* **2010**, *5*, 366−373.

(5) Briseno, A. L.; Holcombe, T. W.; Boukai, A. I.; Garnett, E. C.; Shelton, S. W.; Fréchet, J. M. J.; Yang, P. D. Oligo- and Polythiophene/ZnO Hybrid Nanowire Solar Cells. *Nano Lett.* **2010**, *10*, 334−340.

(6) Lieber, C. M. Semiconductor Nanowires: A Platform for Nanoscience and Nanotechnology. *MRS Bull.* **2011**, *36*, 1052−1063.

(7) Yu, G. H.; Lieber, C. M. Assembly and Integration of Semiconductor Nanowires for Functional Nanosystems. *Pure Appl. Chem.* **2010**, *82*, 2295−2314.

(8) Tian, B. Z.; Lieber, C. M. Design, Synthesis, and Characterization of Novel Nanowire Structures for Photovoltaics and Intracellular Probes. *Pure Appl. Chem.* **2011**, *83*, 2153−2169.

(9) Kempa, T. J.; Cahoon, J. F.; Kim, S.-K.; Day, R. W.; Bell, D. C.; Park, H.-G.; Lieber, C. M. Coaxial Multishell Nanowires with High-Quality Electronic Interfaces and Tunable Optical Cavities for Ultrathin Photovoltaics. *Proc. Natl. Acad. Sci.* **2012**, *109*, 1409−1412.

(10) Tian, Z. R.; Voigt, J. A.; Liu, J.; McDermott, M. J.; Rodriguez, M. A.; Konishi, H.; Xu, H. F. Complex and Oriented ZnO Nanostructures. *Nat. Mater.* **2003**, *2*, 821−826.

(11) Chernova, N. A.; Roppolo, M.; Dillon, A. C.; Whittingham, M. S. Layered Vanadium and Molybdenum Oxide: Batteries and Electrochromics. *J. Mater. Chem.* **2009**, *19*, 2526−2552.

(12) Goodenough, J. B. Cathode Material: A Personal Perspective. *J. Power Sources* **2007**, *174*, 996−1000.

(13) Whittingham, M. S. Lithium Batteries and Cathode Materials. *Chem. Rev.* **2004**, *104*, 4271−4302.

(14) Armand, M.; Tarascon, J.-M. Building Better Batteries. *Nature* **2008**, *451*, 652−657.

(15) Chan, C. K.; Peng, H. L.; Liu, G.; McIlwrath, K.; Zhang, X. F.; Huggins, R. A.; Cui, Y. High-Performance Lithium Battery Anodes Using Silicon Nanowires. *Nat. Nanotechnol.* **2008**, *3*, 31−35.

(16) Kang, B. W.; Ceder, G. Battery Materials for Ultrafast Charging and Discharging. *Nature* **2008**, *458*, 190−193.

(17) Tian, B. Z.; Xie, P.; Kempa, T. J.; Bell, D. C.; Lieber, C. M. Single Crystalline Kinked Semiconductor Nanowire Superstructures. *Nat. Nanotechnol.* **2009**, *4*, 824−829.

(18) Zhang, Q.; Wang, W. S.; Goebl, J.; Yin, Y. D. Self-Templated Synthesis of Hollow Nanostructures. *Nano Today* **2009**, *4*, 494−507.

(19) Ge, J. P.; Zhang, Q.; Zhang, T. R.; Yin, Y. D. Core-Satellite Nanocomposite Catalysts Protected by a Porous Silica Shell: Controllable Reactivity, High Stability, and Magnetic Recyclability. *Angew. Chem., Int. Ed.* **2008**, *47*, 8924−8928.

(20) Shi, S. F.; Cao, M. H.; He, X. Y.; Xie, H. M. Surfactant-Assisted Hydrothermal Growth of Single-Crystalline Ultrahigh-Aspect-Ratio Vanadium Oxide Nanobelts. *Cryst. Growth Des.* **2007**, *7*, 1893−1897.

(21) Mai, L. Q.; Xu, L.; Han, C. H.; Xu, X.; Luo, Y. Z.; Zhao, S. Y.; Zhao, Y. L. Electrospun Ultralong Hierarchical Vanadium Oxide Nanowires with High Performance for Lithium Ion Batteries. *Nano Lett.* **2010**, *10*, 4750−4755.

(22) Mai, L. Q.; Yang, F.; Zhao, Y. L.; Xu, X.; Xu, L.; Luo, Y. Z. Hierarchical MnMoO$_4$/CoMoO$_4$ Heterostructured Nanowires with Enhanced Supercapacitor Performance. *Nat. Commun.* **2011**, *2*, 381−385.

(23) Cao, A. M.; Hu, J. S.; Liang, H. P.; Wan, L. J. Self-Assembled Vanadium Pentoxide (V$_2$O$_5$) Hollow Microspheres from Nanorods and Their Application in Lithium-Ion Batteries. *Angew. Chem., Int. Ed.* **2005**, *44*, 4391−4395.

(24) Liu, J.; Wang, Y.; Peng, Q.; Li, Y. Vanadium Pentoxide Nanobelts: Highly Selective and Stable Ethanol Sensor Materials. *Adv. Mater.* **2005**, *17*, 764−767.

(25) Takeuchi, K. J.; Marschilok, A. C.; Davis, S. M.; Leising, R. A.; Takeuchi, E. S. Silver Vanadium Oxides and Related Battery Applications. *Coord. Chem. Rev.* **2001**, *219*, 283−310.

(26) Liang, C. C.; Bolster, M. E.; Murphy, R. M. *Metal Oxide Composite Cathode Material for High Energy Density Batteries.* U.S. Patent *4310609*, 1982, pp 1−12.

(27) Takeuchi, E. S.; Piliero, P. Lithium/Silver Vanadium Oxide Batteries with Various Silver to Vanadium Ratios. *J. Power Sources* **1987**, *21*, 133−141.

(28) Zhang, S. Y.; Li, W. Y.; Li, C. S.; Chen, J. Synthesis, Characterization, and Electrochemical Properties of $Ag_2V_4O_{11}$ and $AgVO_3$ 1-D Nano/Microstructures. *J. Phys. Chem. B* **2006**, *110*, 24855−24863.

(29) Song, J. M.; Lin, Y. Z.; Yao, H. B.; Fan, F. J.; Li, X. G.; Yu, S. H. Superlong $\beta$-$AgVO_3$ Nanoribbons: High-Yield Synthesis by a Pyridine-Assisted Solution Approach, Their Stability, Electrical and Electrochemical Properties. *ACS Nano* **2009**, *3*, 653−660.

(30) Mai, L. Q.; Xu, X.; Han, C. H.; Luo, Y. Z.; Xu, L.; Wu, Y. M.; Zhao, Y. L. Rational Synthesis of Silver Vanadium Oxides/Polyaniline Triaxial Nanowires with Enhanced Electrochemical Property. *Nano Lett.* **2011**, *11*, 4992−4996.

(31) Rozier, P.; Savariault, J.-M.; Galy, J. $\beta$-$AgVO_3$ Crystal Structure and Relationships with $Ag_2V_4O_{11}$ and $\delta$-$Ag_xV_2O_5$. *J. Solid State Chem.* **1996**, *122*, 303−308.

(32) Jiang, J.; Liu, J. P.; Huang, X. T.; Li, Y. Y.; Ding, R. M.; Ji, X. X.; Hu, Y. Y.; Chi, Q. B.; Zhu, Z. H. General Synthesis of Large-Scale Arrays of One-Dimensional Nanostructured $Co_3O_4$ Directly on Heterogeneous Substrates. *Cryst. Growth Des.* **2010**, *10*, 70−75.

(33) Kokotov, M.; Hods, G. Reliable Chemical Bath Deposition of ZnO Films with Controllable Mmorphology from Ethanolamine-Based Solutions Using $KMnO_4$ Substrate Activation. *J. Mater. Chem.* **2009**, *19*, 3847−3854.

(34) Bao, S. J.; Bao, Q. L.; Li, C. M.; Chen, T. P.; Sun, C. Q.; Dong, Z. L.; Gan, Y.; Zhang, J. Synthesis and Electrical Transport of Novel Channel-Structured $\beta$-$AgVO_3$. *Small* **2007**, *3*, 1174−1177.

(35) Fan, C. L.; Xu, J. K.; Chen, W.; Dong, B. Electrosynthesis and Characterization of Water-Soluble Poly(9-Aminofluorene) with Good Fluorescence Properties. *J. Phys. Chem. C* **2008**, *112*, 12012−12017.

(36) Gabriela, P.; Kissling, C. B.; David, J. F. Tuning Electrochemical Rectification Via Quantum Dot Assemblies. *J. Am. Chem. Soc.* **2010**, *132*, 16855−16861.

(37) Mai, L. Q.; Hu, B.; Chen, W.; Qi, Y. Y.; Lao, C. S.; Yang, R. S.; Dai, Y.; Wang, Z. L. Lithiated $MoO_3$ Nanobelts with Greatly Improved Performance for Lithium Batteries. *Adv. Mater.* **2007**, *19*, 3712−3716.

(38) Mai, L. Q.; Hu, B.; Qi, Y. Y.; Dai, Y.; Chen, W. Improved Cycling Performance of Directly Lithiated $MoO_3$ Nanobelts. *Int. J. Electrochem. Sci.* **2008**, *3*, 216−222.

(39) Delmasa, C.; Cognac-Auradoua, H.; Cocciantellia, J. M.; Menetriera, M.; Doumerca, J. P. The $Li_xV_2O_5$ System: An Overview of the Structure Modifications Induced by the Lithium Intercalation. *Solid State Ionics* **1994**, *69*, 257−264.

(40) Garcia, B.; Millet, M.; Pereira-Ramos, J. P.; Baffier, N.; Bloch, D. Electrochemical Behavior of Chemically Lithiated $Li_xV_2O_5$ phases ($0.9 \leq x \leq 1.6$). *J. Power Sources* **1999**, *81−82*, 670−674.

(41) Lee, S. H.; Kim, Y. H.; Deshpande, R.; Parilla, P. A.; Whitney, E.; Gillaspie, D. T.; Jones, K. M.; Mahan, A.; Zhang, S.; Dillon, A. C. Reversible Lithium-Ion Insertion in Molybdenum Oxide Nanoparticles. *Adv. Mater.* **2008**, *20*, 3627−3632.

(42) Levi, M. D.; Gamolsky, K.; Aurbach, D.; Heider, U.; Oesten, R. Determination of the Li Ion Chemical Diffusion Coefficient for the Topotactic Solid-State Reactions Occurring Via a Two-Phase or Single-Phase Solid Solution Pathway. *J. Electroanal. Chem.* **1999**, *477*, 32−40.

(43) Prosini, P. P.; Lisi, M.; Zane, D.; Pasquali, M. Determination of the Chemical Diffusion Coefficient of Lithium in $LiFePO_4$. *Solid State Ionics* **2002**, *148*, 45−51.